Experimental realization of topological corner states in long-range-coupled electrical circuits

Nikita A. Olekhno [ORCID],* Alina D. Rozenblit [ORCID],* Valerii I. Kachin [ORCID], Alexey A. Dmitriev, Oleg I. Burmistrov, Pavel S. Seregin, Dmitry V. Zhirihin [ORCID], and Maxim A. Gorlach [ORCID]†

School of Physics and Engineering, ITMO University, Saint Petersburg 197101, Russia

Topological corner states are zero-dimensional localized excitations whose existence is protected by the bulk properties of the system. This feature makes them robust to disorder unveiling intriguing physics. Canonical realizations of higher-order topology in two-dimensional systems typically rely on tight-binding models with the nearest-neighbor couplings. Here, in contrast, we propose a D_4-symmetric system where the topological band gap opens due to the additional long-range interactions, which are controllably incorporated in our setup based on a resonant electrical circuit. In our experiments, we probe the response of the designed circuit at every node, reconstruct the eigenmode profiles, and directly extract the topological invariant demonstrating the topological origin of the observed symmetry-protected corner states.

Higher-order topological (HOT) insulators have recently emerged as a distinct class of topological systems [1–3] being implemented experimentally with various platforms, including crystalline solids [4], phononic [5], acoustic [6–8], and electromagnetic setups operating at infrared [9,10] and microwave [11,12] frequencies, as well as resonant electrical circuits [13,14]. The formation of such phases is often governed by the lattice symmetries, with kagome [15] and breathing honeycomb [16] lattices being prominent examples. Due to their ability to confine field in the structures of different dimensionality, HOT phases are promising candidates for topological resonators and lasers [17–20]. In a number of systems, HOT phases are manifested via in-gap corner states. At the same time, higher-order topology can be detected even if the topological state overlaps spectrally with the bulk band [21].

In many cases, the physics of such systems can be understood in terms of tight-binding models involving only the nearest neighbors' interaction. However, this is not the case for photonics, where the long-range interactions of the individual meta-atoms can significantly alter the band structure [12,22].

Recently, several microwave [23,24] and acoustic [25] experiments have demonstrated the emergence of corner states in the two-dimensional (2D) generalization of the celebrated Su-Schrieffer-Heeger (SSH) model with D_4 symmetry [26]. At the same time, the respective tight binding model [Fig. 1(a)] does not feature a zero-energy band gap, and the associated corner state appears in the continuum of the bulk modes [Fig. 1(b)].

In this Letter, we demonstrate that the emergence of zero-energy band-gap hosting corner-localized states in D_4-symmetric systems crucially depends on the next-nearest-neighbor interaction facilitating the formation of an in-gap corner state. To isolate the physics related to the next-nearest-neighbor coupling, we construct a resonant electrical circuit allowing to flexibly control the magnitude of couplings. Besides the retrieval of frequencies and mode profiles for bulk, edge, and corner states, we also reveal the generalized chiral symmetry of the model and extract the topological invariant associated with D_4 lattice symmetry.

Theoretical model. We introduce the *extended* 2D SSH model which differs from the conventional one [Fig. 1(a)] by the presence of additional couplings $M > 0$ between the diagonally opposite next-nearest neighbors, Fig. 1(c). The eigenstates of both conventional and extended 2D SSH models [Figs. 1(a) and 1(c)] are found as the solutions to the eigenvalue problem

$$\sum_{m',n'} H_{mn,m'n'} \beta_{m'n'} = \varepsilon \beta_{mn} , \qquad (1)$$

where the coefficients β_{mn} describe the amplitude of the field at site (m, n), ε is the eigenmode energy defined such that the zero energy corresponds to the resonance frequency of an isolated site, and $\hat{H}$ is the Hamiltonian matrix governing the system's properties. The nonzero elements of the Hamiltonian $-J$, $-K$, and $-M$ correspond to the coupling links between the respective sites (m, n) and (m', n'). For the unit cell choice with intracell couplings J shown in Fig. 1(c), the Bloch Hamiltonian matrix describing one unit cell in the k space takes the following form:

$$\hat{H}(k) = (-1)$$

$$\times \begin{pmatrix} 0 & J + Ke^{-ik_x} & Me^{ik_y - ik_x} & J + Ke^{ik_y} \\ J + Ke^{ik_x} & 0 & J + Ke^{ik_y} & Me^{ik_y + ik_x} \\ Me^{-ik_y + ik_x} & J + Ke^{-ik_y} & 0 & J + Ke^{ik_x} \\ J + Ke^{-ik_y} & Me^{-ik_y - ik_x} & J + Ke^{-ik_x} & 0 \end{pmatrix}$$

$$(2)$$

with the wave vector components k_x, k_y spanning the range $[-\pi, \pi]$ and directed along the x and y axes shown in Fig. 1. The columns of the Hamiltonian matrix from left to right correspond to the unit cell sites with indices A, B, C, and

---

D, respectively. Without loss of generality, we set smaller coupling constant $J = 1$.

Spectrum and eigenstates. Solving the eigenvalue problem Eq. (1), we recover the spectra of 2D SSH models without and with the next-nearest-neighbor couplings M, as shown in Figs. 1(b) and 1(d). Regardless of the ratio K/J, the conventional 2D SSH model is gapless near zero energy, and thus the energy of the corner state appears in the continuum of the bulk modes [Fig. 1(b)]. However, the presence of diagonal couplings M opens a band gap, yielding a spectrally isolated corner-localized state, Fig. 1(d).

It should be stressed that the proposed system [Fig. 1(c)] is the minimal model which captures the effect of long-range interactions in photonic systems since the diagonal links M introduced in the strong-coupling unit cell are the dominant terms related to the interaction of the next-nearest neighbors. Even though the corner state profile shown in the inset of Fig. 1(d) strongly resembles that in the canonical quadrupole insulator [1,27], all the coupling links in our model are positive, which vastly simplifies the experimental implementation of the proposed system.

Hierarchy of the states. To address the localization properties of eigenmodes in the introduced model, we study their *inverse participation ratios* (IPRs) [28]

$$\text{IPR} = \sum_{n,m} |\beta_{mn}|^4, \qquad (3)$$

where the summation is performed over all sites (m, n) of the system with coordinates $1 \leqslant m, n \leqslant N$, and the eigenmode profiles are normalized by the condition $\sum_{n,m} |\beta_{mn}|^2 = 1$. Low values IPR $\rightarrow 0$ correspond to delocalized excitations, while high values IPR $\rightarrow 1$ indicate tight localization.

The results in Fig. 2(a) suggest that the corner state is spectrally isolated only in a certain range of next-nearest-neighbor coupling strengths $M_{\min} < M < M_{\max}$, with $M_{\min} \approx 1.6$ and $M_{\max} \approx 6.3$ for $K = 4$. The corner state profile in such a case is depicted in Fig. 2(b) featuring a pronounced localization at the corner with the weak coupling links J.

The emergence of the corner state in our system is accompanied by the formation of the edge states [Fig. 2(c)] inherited from the conventional 2D SSH model and pinned to the edges terminated by the weak links [29]. Note that the edge states' energy remains unaffected by the additional coupling M as long as the edge states remain confined to the edges where such next-nearest-neighbor couplings are absent, Fig. 2(a).

At the same time, the energies of the bulk modes delocalized over the entire 2D system [Fig. 2(d)] feature a pronounced dependence on M. Besides, they give rise to the states with a stronger localization seen in Fig. 2(a). However, more careful analysis [30] shows that these states are not bound states in the continuum like those in the conventional 2D SSH model [31,32] but rather the states with enhanced localization that still can hybridize with the bulk modes.

Topological properties. Based on the D_4 symmetry of the designed structure, we assess the topological characteristics of our model by checking the behavior of the field profiles under C_2 and C_4 symmetry transformations in few high-symmetry points of the first Brillouin zone [33]. Due to the C_4 symmetry of the lattice, the topological invariant contains three independent components $\chi = (\#X_1^{(2)} - \#\Gamma_1^{(2)}, \#M_1^{(4)} -$
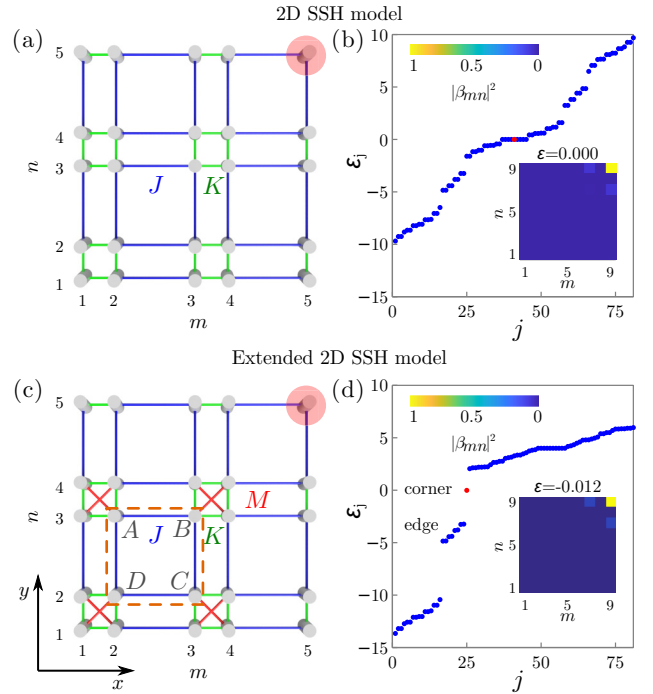

FIG. 1. (a) Schematics of the conventional 2D SSH model realized as an array of coupled cavities with the nearest-neighbor coupling strengths $J > 0$ and $K > J$. (b) Spectrum of energies ε_j versus eigenvalue number j for the model with 9×9 sites from panel (a) with couplings $J = 1$ and $K = 4$. Inset shows the wave function for one of the eigenmodes with ε closest to zero. (c) The proposed extension of 2D SSH model with additional couplings $M > 0$ in the strong-link unit cell. Orange dashed line shows the weak-link unit cell choice used for the analysis of a periodic system. Labels A, B, C, and D denote four sites of the unit cell. (d) Energy spectrum of the model in panel (c) with parameters $J = 1$, $K = M = 4$ having the size of 9×9 sites. Inset shows the field profile of the corner mode. Red shaded area in (a) and (c) highlights the location of the corner state.

$\#\Gamma_1^{(4)}, \#M_2^{(4)} - \#\Gamma_2^{(4)})$, where the upper index denotes the type of the applied rotation operator (C_2 or C_4), the lower index describes the behavior of the wave function under the symmetry transformation, and # denotes the number of eigenstates with a given transformation law below the particular band gap in Γ, M, or X point of the first Brillouin zone.

The considered topological invariant depends on the choice of the unit cell. If the unit cell is chosen with the strong links inside, the invariant is (0,0,0), indicating the absence of topological states at the strong link corner. However, if the unit cell is chosen with weak links inside [Fig. 1(c)], the topological invariant becomes nonzero:

$$\chi = (-1, -1, 0), \qquad (4)$$

heralding the emergence of a corner state with associated corner charge $Q_{\text{corner}} = \frac{1}{4}$ and dipole polarization $\mathbf{P} = (\frac{1}{2}, \frac{1}{2})$ [33]. The calculations are detailed in [30]. It should be stressed that the topological invariant does not depend on M. Nevertheless, the next-nearest-neighbor interaction is crucial to open the band gap at energies close to zero.

It is important to emphasize that the corner state persists in our system even if the D_4 symmetry of the lattice is broken by
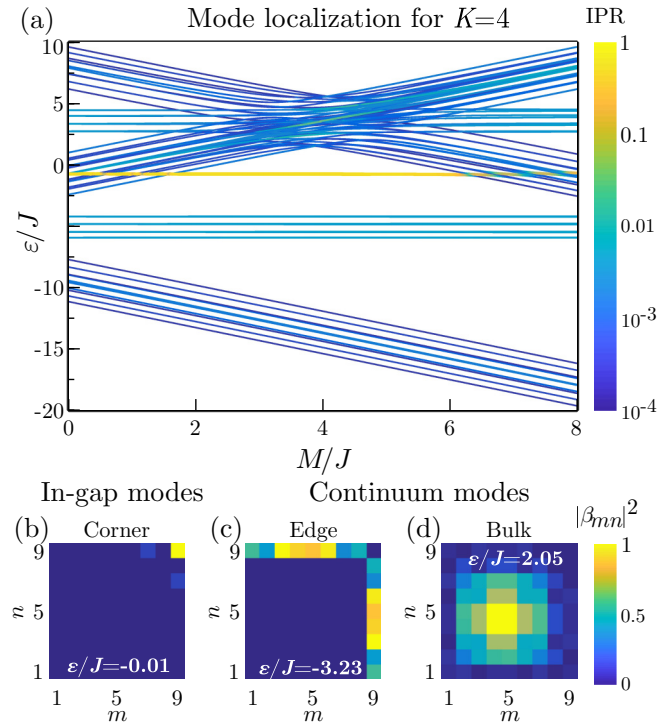
FIG. 2. (a) Energy spectrum of 9×9 structure with coupling constants $J = 1$ and $K = 4$ versus the strength of next-nearest-neighbor coupling M in the range $0 < M < 8$. Color shows the inverse participation ratios (IPR) of the eigenmodes. (b),(c) Eigenmode profiles corresponding to the in-gap corner state (b) and the edge state (c) at $M = 4$. (d) The delocalized bulk state at $M = 4$.
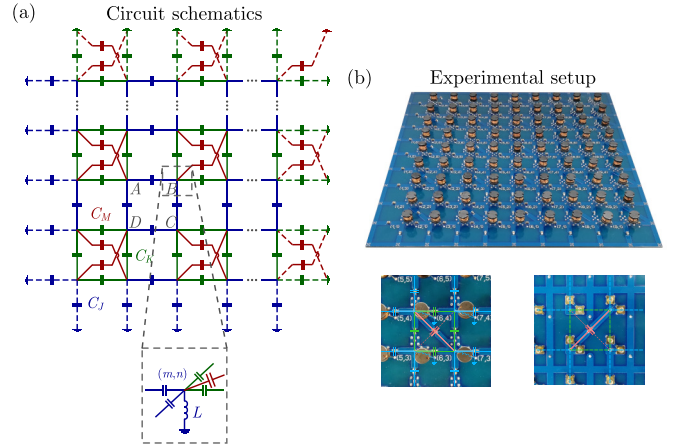

FIG. 3. (a) Equivalent electrical circuit realizing the tight-binding model Fig. 1(c). Each node is grounded by the inductor L and connected to its neighbors via capacitors C_J, C_K, and C_M representing respective tunneling links J, K, and M of the extended 2D SSH model. The boundary nodes of the circuit are grounded with additional elements to provide the exact mapping between the Kirchhoff's rules for the circuit and tight-binding equations. Labels A, B, C, and D denote sites of the unit cell in accordance with Fig. 1(c). (b) The photograph of the experimental setup with 9×9 nodes. Half of the additional diagonal couplings C_M are seen at the top side of circuit along with capacitors C_J, C_K and grounding inductors L, while the remaining couplings C_M are placed at the bottom side carrying also the plugs to connect the measurement equipment. The unit cell of the circuit is shown in the insets at the bottom. The left inset demonstrates top view, while the right inset shows the opposite side of the setup mirrored to show the matching of the bonds.

the appropriate choice of the couplings [30]. This hints that the corner state may arise partly due to the contribution of the edge states band [34]. Our calculations for the semi-infinite geometry indeed reveal nontrivial polarization associated with the band of edge states [30].

Electrical circuit platform. To experimentally confirm that the next-nearest-neighbor couplings M provide the crucial ingredient in the formation of in-gap topological corner state, we need to eliminate the contribution of other long-range couplings that inevitably arise in optical or microwave setups based on resonator arrays. To this end, we construct a topological electrical circuit, Figs. 3(a) and 3(b), in which we can directly control the couplings between the circuit nodes by placing the desired lumped elements. This extreme flexibility in managing the geometry and amplitudes of the couplings in comparison with the other platforms allows applying electrical circuits to emulate such exotic phenomena as four-dimensional quantum Hall phase [35], two-particle topological states of interacting photons [36], and nonlinearity-induced topological states [37] along with the implementation of higher-order topological insulators [13,38,39] and edge states in topological insulators [40], including the conventional 2D SSH model [29].

The construction of electrical circuit is based on the exact correspondence between the tight binding problem Eq. (1) describing the on-site amplitudes β_{mn} and a set of Kirchhoff's rules describing electric potentials φ_{mn} at the respective nodes of the equivalent circuit depicted in Fig. 3(a). The parameters

of the circuit such as capacitances C_J, C_K, C_M, and grounding inductors L on one side and the parameters of tight-binding model on the other are linked as

$$K = \frac{C_K}{C_J}, \quad M = \frac{C_M}{C_J}, \quad \varepsilon = \frac{f_0^2}{f^2} - \left(2 + 2\frac{C_K}{C_J} + \frac{C_M}{C_J}\right), \quad (5)$$

where f is the frequency of the circuit mode, ε is the energy in the tight-binding model, and $f_0 = 1/(2\pi\sqrt{LC_J})$. Thus, ascending energies ε correspond to the descending mode frequencies f in the electrical circuit. To compensate for the absence of neighbors for the boundary nodes of the circuit and maintain the correspondence with the theoretical model, nodes at the edges are grounded with additional elements C_J, C_K, and C_M parallel to the inductors L, in accordance with Fig. 3(a). Further details on electrical circuit model, including the discussion of the boundary conditions, are provided in [30].

The experimental realization of the circuit with $C_J = 1\ \mu F$, $C_K = C_M = 4\ \mu F$, and $L = 23.2\ \mu H$ corresponding to the considered model with $K = M = 4$ and the size of 9×9 sites is shown in Fig. 3(b). Such a circuit has resonances in the kHz frequency range. To probe the modes of the circuit, we apply the external harmonic signal at frequency f with amplitude $U_{ext} = 63$ mV, attaching the signal generator having the series impedance 50 Ω between the given node and ground. Then, we measure the resulting voltage as a function of frequency, which characterizes the circuit impedance.
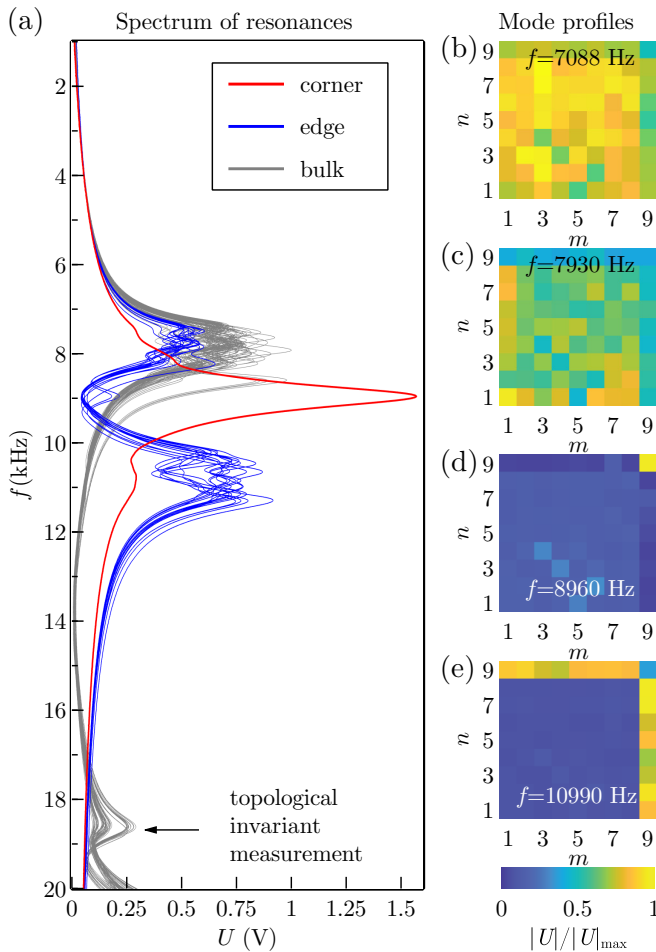
FIG. 4. (a) Resonant response of the circuit measured at every node in the range from 1 to 20 kHz showing the on-site voltages $U(f)$ between the given node (m, n) and ground excited by the external harmonic driving at frequency f with the amplitude $U_{ext} = 63$ mV applied between the corresponding node and ground. Grey curves represent bulk and edge nodes with coordinates $1 \leqslant m, n \leqslant 8$, blue curves correspond to the edge nodes with $1 \leqslant m \leqslant 8, n = 9$, and $1 \leqslant n \leqslant 8, m = 9$, the red curve represents the corner node $m = 9, n = 9$. The arrow points towards the frequency $f = 18\,616$ Hz at which the topological invariant is retrieved. (b)–(e) Spatial maps of the on-site voltage responses to the external excitation $U_{ext} = 63$ mV at a given frequency f representing bulk (b),(c), corner (d), and edge (e) states of the extended 2D SSH model. Color shows the absolute value of voltage between the node (m, n) and ground normalized by its maximal value calculated for each map separately.

Resonant response of the circuit. The impedance spectra at bulk circuit nodes shown in Fig. 4(a) by gray lines exhibit a band gap between 9 and 18 kHz. This band gap is occupied by the modes with frequencies 10–12 kHz localized at the edges of the circuit, and a single mode pinned to the node (9,9) with the frequency around 9 kHz. Attaching a harmonic

signal generator to every node of the circuit and measuring the voltages between the given node (m, n) and the ground at the fixed frequency f, we recover voltage maps shown in Figs. 4(b)–4(e). As seen from these maps, the respective modes represent bulk, edge, and corner states in the considered extended 2D SSH model and their measured frequencies agree with the predictions of the tight-binding model. The detected corner mode reveals the topological origin of our system. To support this conclusion further, we retrieve the topological invariant directly from the experimental data as outlined in Ref. [30].

The peaks in the spectrum experience considerable broadening caused by ohmic losses in the inductors and wires of the printed circuit board. Another reason for broadening is the spread in lumped elements' values, as discussed in [30]. It should be stressed that the in-gap corner state Fig. 4(d) possesses the largest Q factor compared to the other resonances in the circuit, reaching $Q \approx 10$. It also remains nearly unperturbed even in the presence of losses and disorder in the component values in contrast to the corner state in continuum [Fig. 4(c); see [30] for details] which strongly hybridizes with the bulk modes [Fig. 4(b)].

The above robustness is especially interesting since the fluctuations in the values of capacitors in the circuit simultaneously induce off-diagonal and diagonal disorder. Nevertheless, the experimental results demonstrate an excellent agreement with the theoretical predictions even in the presence of disorder and dissipation for a system size small as 9×9 sites which is explained by the significant band-gap width compared to the magnitude of disorder. These results highlight the potential of topological corner states in constructing small-scale photonic [41] and electronic devices.

Conclusion. We have demonstrated the crucial role played by the next-nearest-neighbor interaction in the formation of topological corner states in D_4-symmetric systems. While the conventional 2D SSH model is gapless at zero energy, even a small interaction of the next-nearest neighbors opens the topological band gap. Thus, our results provide a clear physical interpretation of the corner states observed in recent experiments with the arrays of microwave resonators [23,24] and acoustic metamaterials [25]. Furthermore, our study reveals the fundamental role of long-range interactions in the formation of topological phases and further highlights the potential of resonant electrical circuits in probing topological states and phases.

[1] W. A. Benalcazar, B. A. Bernevig, and T. L. Hughes, Quantized electric multipole insulators, Science **357**, 61 (2017).

[2] F. Schindler, A. M. Cook, M. G. Vergniory, Z. Wang, S. S. P. Parkin, B. A. Bernevig, and T. Neupert, Higher-order topological insulators, Sci. Adv. **4**, eaat0346 (2018).

[3] B. Xie, H.-X. Wang, X. Zhang, P. Zhan, J.-H. Jiang, M. Lu, and Y. Chen, Higher-order band topology, Nat. Rev. Phys. **3**, 520 (2021).

[4] F. Schindler, Z. Wang, M. G. Vergniory, A. M. Cook, A. Murani, S. Sengupta, A. Yu. Kasumov, R. Deblock, S. Jeon, I. Drozdov, H. Bouchiat, S. Guéron, A. Yazdani, B. A. Bernevig, and T. Neupert, Higher-order topology in bismuth, Nat. Phys. **14**, 918 (2018).

[5] M. Serra-Garcia, V. Peri, R. Süsstrunk, O. R. Bilal, T. Larsen, L. G. Villanueva, and S. D. Huber, Observation of a phononic quadrupole topological insulator, Nature (London) **555**, 342 (2018).

[6] H. Xue, Y. Yang, F. Gao, Y. Chong, and B. Zhang, Acoustic higher-order topological insulator on a kagome lattice, Nat. Mater. **18**, 108 (2019).

[7] X. Ni, M. Weiner, A. Alù, and A. B. Khanikaev, Observation of higher-order topological acoustic states protected by generalized chiral symmetry, Nat. Mater. **18**, 113 (2019).

[8] Z. Zhang, Y. Tian, Y. Wang, S. Gao, Y. Cheng, X. Liu, and J. Christensen, Directional acoustic antennas based on valley-hall topological insulators, Adv. Mater. **30**, 1803229 (2018).

[9] S. Mittal, V. V. Orre, G. Zhu, M. A. Gorlach, A. Poddubny, and M. Hafezi, Photonic quadrupole topological phases, Nat. Photonics **13**, 692 (2019).

[10] A. E. Hassan, F. K. Kunst, A. Moritz, G. Andler, E. J. Bergholtz, and M. Bourennane, Corner states of light in photonic waveguides, Nat. Photonics **13**, 697 (2019).

[11] C. W. Peterson, W. A. Benalcazar, T. L. Hughes, and G. Bahl, A quantized microwave quadrupole insulator with topologically protected corner states, Nature (London) **555**, 346 (2018).

[12] M. Li, D. Zhirihin, M. Gorlach, X. Ni, D. Filonov, A. Slobozhanyuk, A. Alù, and A. B. Khanikaev, Higher-order topological states in photonic kagome crystals with long-range interactions, Nat. Photonics **14**, 89 (2020).

[13] S. Imhof, C. Berger, F. Bayer, J. Brehm, L. W. Molenkamp, T. Kiessling, F. Schindler, C. H. Lee, M. Greiter, T. Neupert, and R. Thomale, Topolectrical-circuit realization of topological corner modes, Nat. Phys. **14**, 925 (2018).

[14] M. Serra-Garcia, R. Süsstrunk, and S. D. Huber, Observation of quadrupole transitions and edge mode topology in an LC circuit network, Phys. Rev. B **99**, 020304(R) (2019).

[15] A. Vakulenko, S. Kiriushechkina, M. Wang, M. Li, D. Zhirihin, X. Ni, S. Guddala, D. Korobkin, A. Alù, and A. B. Khanikaev, Near-field characterization of higher-order topological photonic states at optical frequencies, Adv. Mater. **33**, 2004376 (2021).

[16] L.-H. Wu and X. Hu, Scheme for Achieving a Topological Photonic Crystal by Using Dielectric Material, Phys. Rev. Lett. **114**, 223901 (2015).

[17] B. Bahari, A. Ndao, F. Vallini, A. E. Amili, Y. Fainman, and B. Kanté, Nonreciprocal lasing in topological cavities of arbitrary geometries, Science **358**, 636 (2017).

[18] W. Zhang, X. Xie, H. Hao, J. Dang, S. Xiao, S. Shi, H. Ni, Z. Niu, C. Wang, K. Jin, X. Zhang, and X. Xu, Low-threshold topological nanolasers based on the second-order corner state, Light Sci. Appl. **9**, 109 (2020).

[19] C. Han, M. Kang, and H. Jeon, Lasing at multidimensional topological states in a two-dimensional photonic crystal structure, ACS Photonics **7**, 2027 (2020).

[20] H.-R. Kim, M.-S. Hwang, D. Smirnova, K.-Y. Jeong, Y. Kivshar, and H.-G. Park, Multipolar lasing modes from topological corner states, Nat. Commun. **11**, 5758 (2020).

[21] C. W. Peterson, T. Li, W. A. Benalcazar, T. L. Hughes, and G. Bahl, A fractional corner anomaly reveals higher-order topology, Science **368**, 1114 (2020).

[22] Y. Chen, F. Meng, Z. Lan, B. Jia, and X. Huang, Dual-Polarization Second-Order Photonic Topological Insulators, Phys. Rev. Appl. **15**, 034053 (2021).

[23] X.-D. Chen, W.-M. Deng, F.-L. Shi, F.-L. Zhao, M. Chen, and J.-W. Dong, Direct Observation of Corner States in Second-Order Topological Photonic Crystal Slabs, Phys. Rev. Lett. **122**, 233902 (2019).

[24] B.-Y. Xie, G.-X. Su, H.-F. Wang, H. Su, X.-P. Shen, P. Zhan, M.-H. Lu, Z.-L. Wang, and Y.-F. Chen, Visualization of Higher-Order Topological Insulating Phases in Two-Dimensional Dielectric Photonic Crystals, Phys. Rev. Lett. **122**, 233903 (2019).

[25] Z. Zhang, H. Long, C. Liu, C. Shao, Y. Cheng, X. Liu, and J. Christensen, Deep-subwavelength holey acoustic second-order topological insulators, Adv. Mater. **31**, 1904682 (2019).

[26] F. Liu and K. Wakabayashi, Novel Topological Phase with a Zero Berry Curvature, Phys. Rev. Lett. **118**, 076803 (2017).

[27] W. A. Benalcazar, B. A. Bernevig, and T. L. Hughes, Electric multipole moments, topological multipole moment pumping, and chiral hinge states in crystalline insulators, Phys. Rev. B **96**, 245115 (2017).

[28] D. J. Thouless, Electrons in disordered systems and the theory of localization, Phys. Rep. **13**, 93 (1974).

[29] S. Liu, W. Gao, Q. Zhang, S. Ma, L. Zhang, C. Liu, Y. J. Xiang, T. J. Cui, and S. Zhang, Topologically protected edge state in two-dimensional Su-Schrieffer-Heeger circuit, Research **2019**, 8609875 (2019).

[30] See Supplemental Material at http://link.aps.org/supplemental/10.1103/PhysRevB.105.L081107 for (i) the details of theoretical model; (ii) discussion of generalized chiral symmetry; (iii) theoretical calculation of the topological invariant; (iv) evaluation of edge polarization; (v) analysis of localized states in the continuum; (vi) derivation of the equations for the electrical circuit; (vii) details of the experimental setup; (viii) description of local density of states measurement; (ix) numerical simulations of the designed circuit; (x) retrieval of the topological invariant from the experimental data.

[31] W. A. Benalcazar and A. Cerjan, Bound states in the continuum of higher-order topological insulators, Phys. Rev. B **101**, 161116(R) (2020).

[32] A. Cerjan, M. Jürgensen, W. A. Benalcazar, S. Mukherjee, and M. C. Rechtsman, Observation of a Higher-Order Topological Bound State in the Continuum, Phys. Rev. Lett. **125**, 213901 (2020).

[33] W. A. Benalcazar, T. Li, and T. L. Hughes, Quantization of fractional corner charge in C_n-symmetric higher-order topological crystalline insulators, Phys. Rev. B **99**, 245151 (2019).

[34] M. Jung, Y. Yu, and G. Shvets, Exact higher-order bulk-boundary correspondence of corner-localized states, Phys. Rev. B **104**, 195437 (2021).

[35] Y. Wang, H. M. Price, B. Zhang, and Y. D. Chong, Circuit implementation of a four-dimensional topological insulator, Nat. Commun. **11**, 2356 (2020).

[36] N. A. Olekhno, E. I. Kretov, A. A. Stepanenko, P. A. Ivanova, V. V. Yaroshenko, E. M. Puhtina, D. S. Filonov, B. Cappello, L. Matekovits, and M. A. Gorlach, Topological edge states of interacting photon pairs emulated in a topolectrical circuit, Nat. Commun. **11**, 1436 (2020).

[37] Y. Hadad, J. C. Soric, A. B. Khanikaev, and A. Alù, Self-induced topological protection in nonlinear circuit arrays, Nat. Electron. **1**, 178 (2018).

[38] J. Bao, D. Zou, W. Zhang, W. He, H. Sun, and X. Zhang, Topo-electrical circuit octupole insulator with topologically protected corner states, Phys. Rev. B **100**, 201406(R) (2019).

[39] S. Liu, S. Ma, Q. Zhang, L. Zhang, C. Yang, O. You, W. Gao, Y. Xiang, T. J. Cui, and S. Zhang, Octupole corner state in a three-dimensional topological circuit, Light Sci. Appl. **9**, 145 (2020).

[40] J. Ningyuan, C. Owens, A. Sommer, D. Schuster, and J. Simon, Time- and Site-Resolved Dynamics in a Topological Circuit, Phys. Rev. X **5**, 021031 (2015).

[41] D. V. Zhirihin and Y. S. Kivshar, Topological photonics on a small scale, Small Science **1**, 2100065 (2021).